Dynamic stability with the disturbance-free payload architecture as applied to the Large UV/Optical/Infrared (LUVOIR) Mission

Larry D. Dewell, Kiarash Tajdaran, Raymond M. Bell, Kuo-Chia Liu, Matthew R. Bolcar, et al.

Larry D. Dewell, Kiarash Tajdaran, Raymond M. Bell, Kuo-Chia Liu, Matthew R. Bolcar, Lia W. Sacks, Julie A. Crooke, Carl Blaurock, "Dynamic stability with the disturbance-free payload architecture as applied to the Large UV/Optical/Infrared (LUVOIR) Mission," Proc. SPIE 10398, UV/Optical/IR Space Telescopes and Instruments: Innovative Technologies and Concepts VIII, 103980B (5 September 2017); doi: 10.1117/12.2274287

Event: SPIE Optical Engineering + Applications, 2017, San Diego, California, United States

Dynamic Stability with the Disturbance-Free Payload Architecture as Applied to the Large UV/Optical/Infrared (LUVOIR) Mission

Larry D. Dewell[1*a], Kiarash Tajdaran[a], Raymond M. Bell[a], Kuo-Chia Liu[b], Matthew R. Bolcar[b], Lia W. Sacks[b], Julie A. Crooke[b], Carl Blaurock[c],
[a]Lockheed Martin Space Systems Company, Advanced Technology Center, 3251 Hanover St., Palo Alto, CA, USA 94304; [b]NASA Goddard Space Flight Center, Attitude Control Systems, 8800 Greenbelt Rd., Code 591, Greenbelt, MD USA 20771; [c]Nightsky Systems Inc., 3916 Lauriston Rd., Raleigh, NC USA 27616

ABSTRACT

The need for high payload dynamic stability and ultra-stable mechanical systems is an overarching technology need for large space telescopes such as the Large Ultraviolet / Optical / Infrared (LUVOIR) Surveyor. Wavefront error stability of less than 10 picometers RMS of uncorrected system WFE per wavefront control step represents a drastic performance improvement over current space-based telescopes being fielded. Previous studies of similar telescope architectures have shown that passive telescope isolation approaches are hard-pressed to meet dynamic stability requirements and usually involve complex actively-controlled elements and sophisticated metrology. To meet these challenging dynamic stability requirements, an isolation architecture that involves no mechanical contact between telescope and the host spacecraft structure has the potential of delivering this needed performance improvement. One such architecture, previously developed by Lockheed Martin called Disturbance Free Payload (DFP), is applied to and analyzed for LUVOIR. In a non-contact DFP architecture, the payload and spacecraft fly in close proximity, and interact via non-contact actuators to allow precision payload pointing and isolation from spacecraft vibration. Because disturbance isolation through non-contact, vibration isolation down to zero frequency is possible, and high-frequency structural dynamics of passive isolators are not introduced into the system. In this paper, the system-level analysis of a non-contact architecture is presented for LUVOIR, based on requirements that are directly traceable to its science objectives, including astrophysics and the direct imaging of habitable exoplanets. Aspects of architecture and how they contribute to system performance are examined and tailored to the LUVOIR architecture and concept of operation.

Keywords: LUVOIR, non-contact, vibration isolation, ultra-stable, disturbance-free payload

1. LUVOIR AND TELESCOPE DYNAMIC STABILITY

The Large UV/Optical/IR Surveyor (LUVOIR) is a concept for a highly capable, multi-wavelength space observatory with ambitious science goals. This mission would enable great leaps forward in a broad range of science, from the epoch of reionization, through galaxy formation and evolution, star and planet formation, to solar system remote sensing[1]. LUVOIR as an observatory will have broad science capabilities, spanning the Far-UV to Near-IR bandpass. The ambitious science goals of LUVOIR impose stringent requirements on the dynamic stability of the telescope mechanical structure. Since the primary telescope disturbance source arises from the spacecraft (such as control-moment gyroscopes or thrusters), stringent requirements on telescope dynamic stability imply strong levels of vibration isolation of spacecraft disturbances. This section will describe the LUVOIR architecture, and trace science objectives down to telescope vibration isolation.

1.1 LUVOIR Mission Overview and Telescope Pointing Architecture

The candidate LUVOIR architecture considered in this paper involves a 15-meter segmented Primary mirror aperture. The suite of imagers and spectrographs in this architecture include: (a) Optical / NIR High-contrast (1010) Coronagraph; (b) UV Multi-object Spectrograph & Imager (LUMOS); (c) NUV / Optical / NIR Wide-field Camera (HDI); (d) Optical / NIR Multi-resolution Spectrograph (O/NIRS). LUVOIR is designed to operate at the Earth-Sun L2 point, and be serviceable, with a 5-year minimum lifetime for consumables and instruments. The overall LUVOIR observatory is shown in Figure 1.

* larry.dewell@lmco.com; phone 1 650-424-2706; http://www.lockheedmartin.com/us/ssc/atc.html

UV/Optical/IR Space Telescopes and Instruments: Innovative Technologies and Concepts VIII
edited by Howard A. MacEwen, James B. Breckinridge, Proc. of SPIE Vol. 10398, 103980B
 · doi: 10.1117/12.2274287

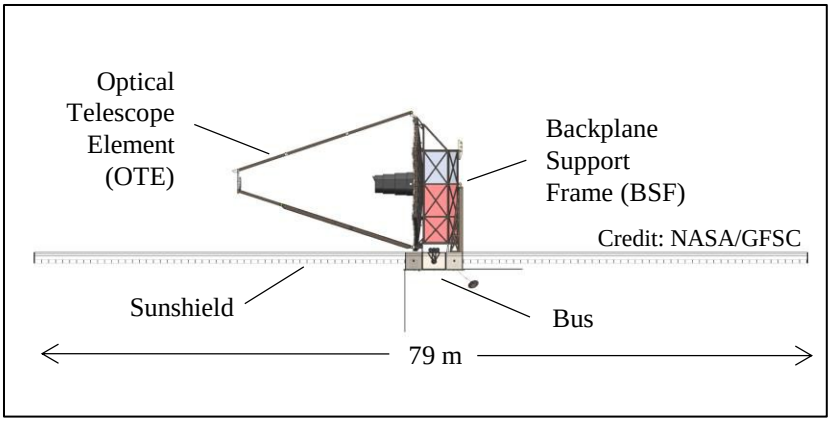

Figure 1. The 15-meter LUVOIR Observatory architecture.

The major components of the Backplane Support Frame (BSF) are shown in Figure 2. A 2-DOF gimbal mechanism allows for pointing of the telescope relative to the rest of the observatory. Outboard of the gimbal, a Vibration Isolation and Precision Pointing System (VIPPS) is system that connects the payload to the spacecraft, and simultaneously provides vibration isolation and pointing. For the purposes of this paper, the LUVOIR "payload" body comprises the entire assembly of components that are outboard of the 2-DOF gimbal (including the telescope, optical bench and other components), and the "spacecraft" body comprises the remainder of integrated spacecraft structure that is inboard of the 2-DOF gimbal, including the gimbal mechanism itself.

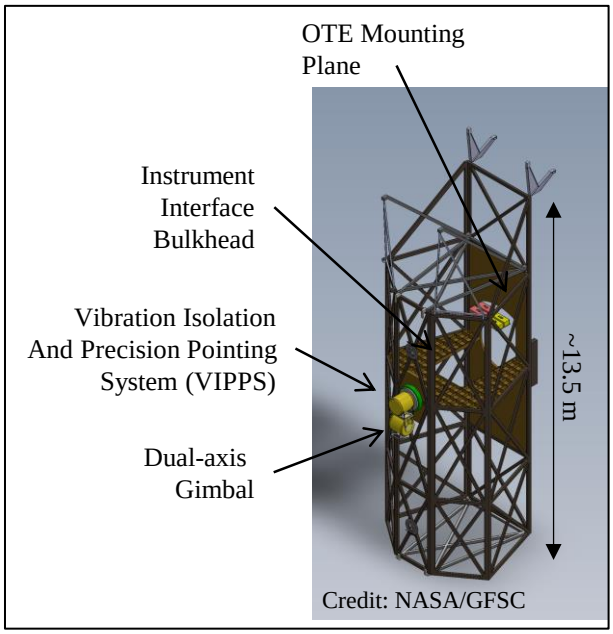

Figure 2. The LUVOIR Backplane Support Frame (BSF).

During a long-duration science observations, LUVOIR employs a cascaded control architecture to precisely control telescope line-of-sight while also managing the limited stroke of actuators and mechanisms. Figure 3 shows a block diagram of this cascaded control architecture. The innermost control loop uses a Fine Steering Mirror (FSM) and low-order wavefront sensor. A separate loop uses measurements of LOS error to drive the VIPPS actuators to control overall Payload LOS at a lower bandwidth, thus keeping the FSM within its operational range. Finally, the VIPPS interface sensors drive the inertial attitude control actuators of the spacecraft to keep the VIPPS within its operational range.

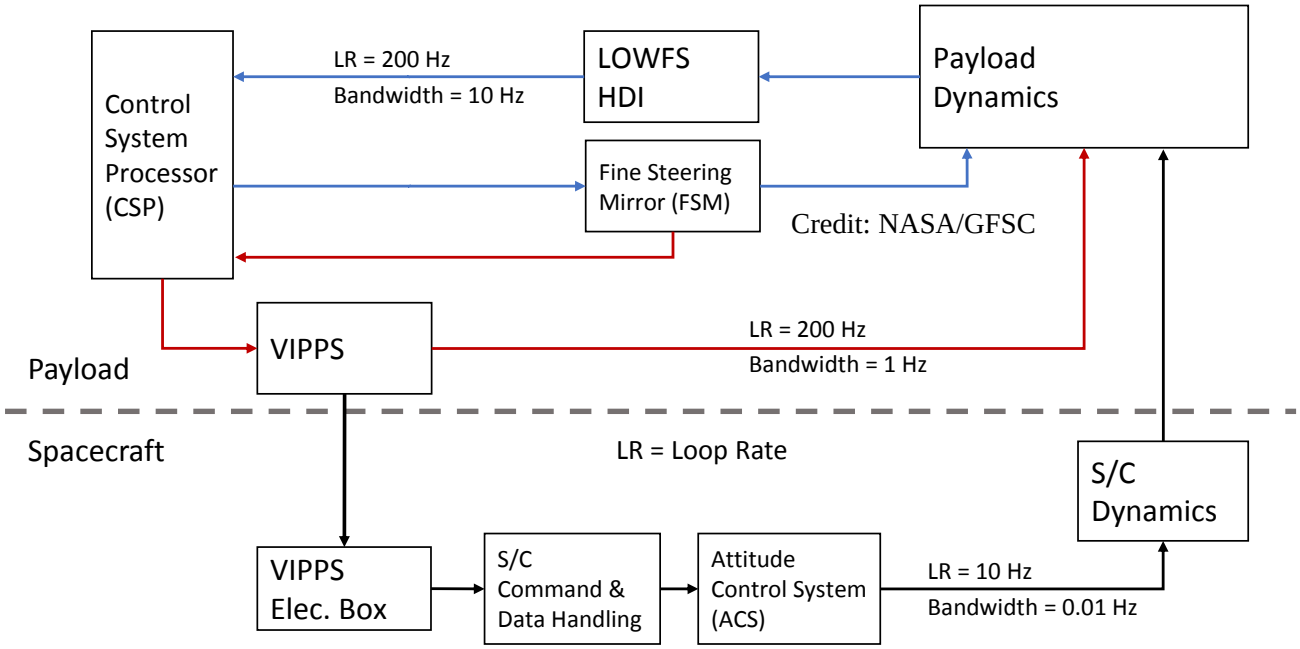

Figure 3. The LUVOIR control system architecture during science observation.

1.2 Driving Requirements for Telescope Dynamic Stability

High temporal stability of the dark hole contrast for the LUVOIR coronograph requires stable wavefront error (WFE) between wavefront sensing and control steps. Due to the low WFE sensing and control sample rate (about 10 minutes), this requirement results in extreme WFE stability: less than 10 picometers RMS WFE over about 10 minutes. WFE arises from rigid-body motion of the optics within the instrument assembly, primary mirror segment relative motion (piston, tip and tilt) and primary-secondary relative motion. The relative motion of these optical and structural elements is largely driven by mechanical disturbances arising from observatory observations: operation of spacecraft attitude control actuators (such as control-moment gyroscopes), spacecraft thrusters during stationkeeping or momentum management, and any other moving mechanisms, such as communication antennas. In addition to extremely low WFE stability, LUVOIR requires very low residual LOS motion between WFE control steps, driven by requirements from both the coronagraph and the HDI instrument: the LUVOIR architecture considered here requires 0.34 masec RMS LOS stability. LOS stability is also driven by system mechanical disturbances. Thus, in order to meet both the simultaneous and stringent WFE and LOS stability requirements, extremely high isolation performance is required from VIPPS.

In addition to steady-state WFE and LOS stability requirements, LUVOIR had requirements on angular agility. The observatory must be able to slew 3.0 degrees in 60 seconds; this agility requirement limits the lost observing time due to slewing between science targets. Secondly, the observatory must support steady-state angle tracking of moving targets of up to 60 masec/sec; this tracking requirement is derived from performing science against solar system targets. Any isolation system should ideally be capable of supporting these agility requirements without latching or otherwise changing its isolation performance level.

2. NON-CONTACT PAYLOAD VIBRATION ISOLATION

2.1 Disturbance Free Payload (DFP) architecture

In an attempt to achieve the level of vibration isolation from spacecraft disturbances required, LUVOIR is assessing a non-contact implementation for VIPPS. NASA and Lockheed Martin have been pursuing Cooperative Research in 2017, with the specific goal of realizing a non-contact interface. Lockheed Martin has developed and patented a Disturbance Free Payload (DPF) non-contact architecture[2]. DFP is an entirely novel approach for isolating a sensitive science payload from

the supporting spacecraft. *A DFP-configured observatory is actually two physically-separated bodies flying in close formation, and exchanging forces and torques through non-contact actuators.* The DFP control architecture is summarized graphically in Figure 4. The payload controls its rigid-body degrees of freedom (ideally, 6 translational and rotational degrees of freedom, as shown in Figure 4) by pushing against the spacecraft mass and inertia using a set of six non-contact Lorentz force actuators (such as voice coil actuators) with sufficiently large gap that allows for non-contact over the required operational translational and rotational stroke of the interface. The spacecraft in turn controls its rigid-body degrees of freedom such that interface stroke and gap are maintained. With such an architecture, requirements for spacecraft attitude control are no more stringent than those for conventional spacecraft, and do not derive from payload pointing requirements. Because of the DFP control architecture, Payload isolation from Spacecraft disturbances is broadband, even down to low frequency, and is not affected by interface measurement noise. The DFP isolation architecture was assessed for the Terrestrial Planet Finder Coronagraph, where substantial performance margin against coronagraph-derived dynamic stability requirements were predicted with DFP, using integrated structure/controls/optics modeling [3].

As a practical matter, it is not generally practicable to realize a DFP architecture in the payload translational degrees of freedom, because whereas spacecraft inertial attitude control actuators do not involve consumables, inertial spacecraft translation control involves thrusters which consume propellant. In this case, the DFP architecture of Figure 4 is modified so that relative translation control is performed at the non-contact interface; this modified architecture, which will be the focus of this paper, is shown in Figure 5. In this architecture, the non-contact interface sensors are combined to extract an estimate of the interface relative translation degrees of freedom, and this estimate is used to compute interface translation force commands. This architecture introduces low-frequency coupling that does not exist in the 6-DOF architecture of Figure 4, but occurs only in the payload translation degrees of freedom, which do not directly couple into telescope performance.

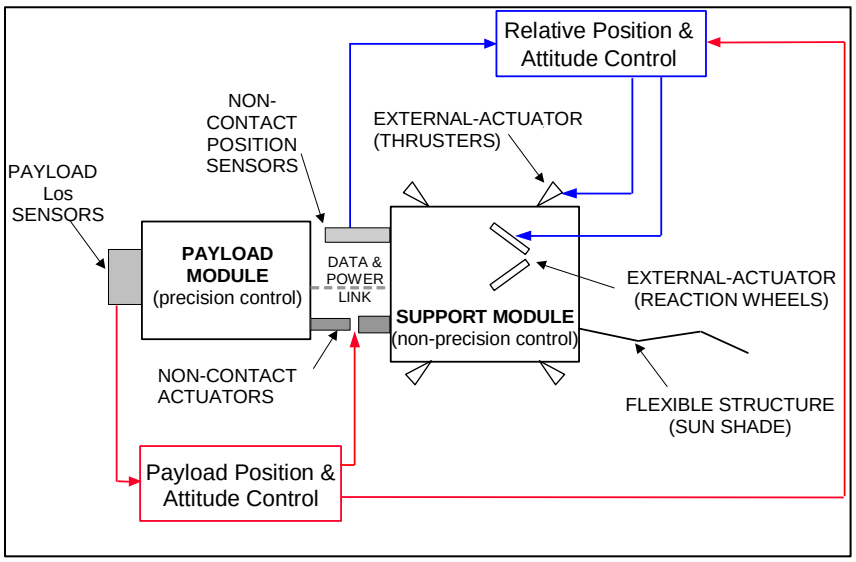

Figure 4. The Disturbance-Free Payload (DFP) control architecture.

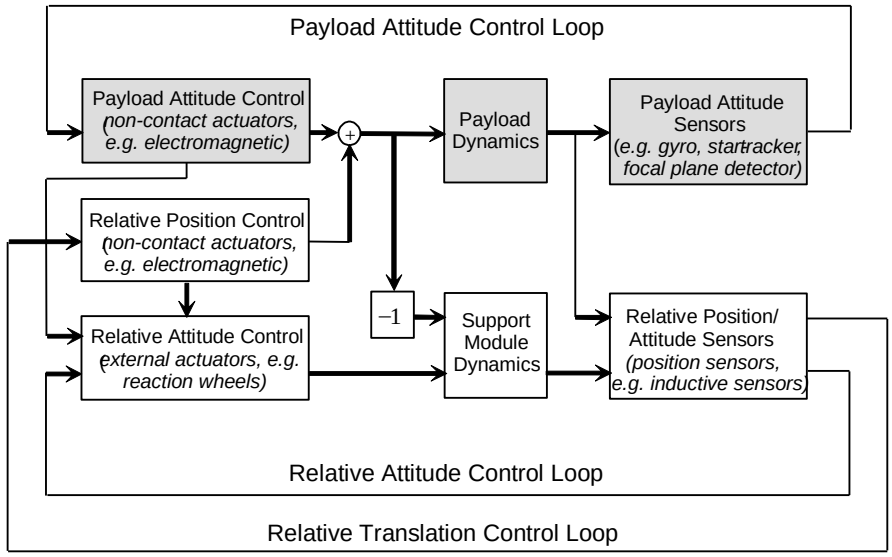

Figure 5. A DFP control architecture where relative translation control is realized using the non-contract actuators.

2.2 Non-contact linear dynamics

In order to perform an initial quantitative isolation performance assessment for LUVOIR, we require the linear rigid-body equations of motion of the payload and spacecraft, with a non-contact interface between them. A linear dynamic assumption is valid during steady-state science observations, where small motion assumptions are valid. The linear analysis here is largely similar to analysis already published by Pedreiro [4]. Let the pair of three-dimensional vectors (ρ_P, θ_P) represent the differential position and attitude of the center-of-mass of the payload from some nominal state, and let (ρ_S, θ_S) be the analogous quantities for the spacecraft. Forces and torques applied to the payload at an interface point (denoted by *I*) can be defined as follows: L^I_{PO} is the force/torque vector arising from controlled actuation of the non-contact actuators, L^I_{PC} is the force/torque vector arising from cables that bridge the interface, and L^I_{PA} is the force/torque vector arising from residual coupling from the non-contact actuators themselves. In addition to these interface forces and torques, let E^C_P and E^C_S denote the force/torque vectors applied at the payload and spacecraft centers-of-mass, respectively, due to disturbances, and let L^C_{SO} denote the controlled force/torque applied to the spacecraft center-of-mass from DFP control. Then the linearized rigid-body equations of motion for the spacecraft and payload are:

$$\begin{bmatrix} M_P & 0 \\ 0 & I_P \end{bmatrix} \begin{bmatrix} \ddot{\rho}_P \\ \ddot{\theta}_P \end{bmatrix} = N_P \left(L^I_{PO} + L^I_{PC} + L^I_{PA} \right) + E^C_P$$
$$\begin{bmatrix} M_S & 0 \\ 0 & I_S \end{bmatrix} \begin{bmatrix} \ddot{\rho}_S \\ \ddot{\theta}_S \end{bmatrix} = N_S \left(-L^I_{PO} - L^I_{PC} - L^I_{PA} \right) + L^C_{SO} + E^C_S \tag{1}$$

where (M_P, I_P) are the 3x3 central mass and inertia matrices of the payload (and analogously for (M_S, I_S)), and (N_P, N_S) are the matrices that transform force/torque applied at interface point *I* to the payload and spacecraft center-of-mass, respectively.

2.3 DFP non-contact control models

The DFP control architecture operates on measurements (or estimates) of the payload attitude, θ_P, the interface relative position, $\rho_R = \rho_P - \rho_S$, and the interface relative attitude, $\theta_R = \theta_P - \theta_S$. The measurements differ from their truth counterparts by measurement (or estimation) noise, as:

$$\hat{\theta}_R = \theta_R + \tilde{\theta}_R \; ; \hat{\rho}_R = \rho_R + \tilde{\rho}_R \; ; \hat{\theta}_P = \theta_P + \tilde{\theta}_P \tag{2}$$

The DFP control architecture with interface relative translation control can be described mathematically in the frequency (Laplace) domain by the following two equations:

$$\begin{aligned} N_P L_{PO}^I &= \begin{bmatrix} -K_\rho(s)\hat{\rho}_R \\ -K_{P\theta}(s)\hat{\theta}_P \end{bmatrix} \\ L_{SO}^C &= \begin{bmatrix} 0 \\ -K_{S\theta}(s)\hat{\theta}_R \end{bmatrix} \end{aligned} \tag{3}$$

In equation (3), the variable *s* is the Laplace frequency-domain variable. The first equation specifies that L_{PO}^I, when transformed into an equivalent force/torque at the payload center-of-mass, decouples into a feedback compensator in the translation degrees of freedom operating on an estimate of the interface relative translation $(\hat{\rho}_R)$, and separate feedback compensator in the rotational degrees of freedom operating on an estimate of the payload inertial attitude $(\hat{\theta}_P)$. This first equation implies that the feedback compensators for payload inertial attitude and interface relative translation utilize a priori knowledge of the location of the interface point relative to the payload center-of-mass. The second equation in (3) states that the inertial control torque applied to the spacecraft is a feedback compensator on an estimate of the interface relative attitude $(\hat{\theta}_R)$.

2.4 System closed-loop dynamics and observations

The estimated quantities $\hat{\rho}_R$ and $\hat{\theta}_P$ are equal to their true counterparts, plus additive random estimation error:

$$\begin{aligned} \hat{\rho}_R &= \rho_R + \tilde{\rho}_R ; \hat{\theta}_P = \theta_P + \tilde{\theta}_P \\ \rho_R &= \rho_P - \rho_S \end{aligned} \tag{4}$$

Although the interface is non-contact in its mechanical design, small coupling effects are assumed in this analysis. The two principal coupling terms modeled here are the presence of power and/or data cables that bridge the interface, and dissipative damping coming from the non-contact voice coil actuators. Linear models for these two coupling effects are expressed mathematically in the frequency domain as:

$$\begin{aligned} L_{PC}^I &= -C\begin{bmatrix} \rho_P - \rho_S \\ \theta_P - \theta_S \end{bmatrix} = -C\begin{bmatrix} \rho_R \\ \theta_R \end{bmatrix} \\ L_{PA}^I &= -As\begin{bmatrix} \rho_R \\ \theta_R \end{bmatrix} \end{aligned} \tag{5}$$

where the 6x6 matrices A and C are the cable stiffness and actuator damping matrices, respectively. Taking the Laplace transform of the equations of motion of (1), and using the DFP controller expressions of (2) and the coupling models of (5), one can derive the closed-loop rigid-body system dynamics in the following frequency-domain form:

$$\left\{\begin{bmatrix} M_P s^2 K_\rho(s) & 0 \\ 0 & I_P s^2 + K_{P\theta}(s) \end{bmatrix} + N_P(As + C)\right\}\begin{bmatrix} \rho_P \\ \theta_P \end{bmatrix} = \begin{bmatrix} K_\rho(s)\rho_S \\ 0 \end{bmatrix} - \begin{bmatrix} K_\rho(s)\tilde{\rho}_R \\ 0 \end{bmatrix} - \begin{bmatrix} 0 \\ K_{P\theta}(s)\tilde{\theta}_P \end{bmatrix} + N_P(As + C)\begin{bmatrix} \rho_S \\ \theta_S \end{bmatrix} + E_P^C \quad (6)$$

From equation (6), several important observations regarding the closed-loop dynamics can be made. First, interface relative translation control does not couple into payload attitude dynamics, by virtue of the DFP controller design. Second, the payload closed-loop attitude dynamics is only weakly coupled to spacecraft attitude dynamics through small interface coupling terms, as represented by the matrices *A* and *C*; section 3 below will explore the sensitivity of interface isolation performance to these small residual coupling terms. Third, payload closed-loop attitude is only driven by payload attitude (line-of-sight) measurement noise, a precision observatory measurement derived from a fine guidance camera, and is independent of interface measurement noise.

3. ISOLATION TRANSMISSIBILITY PERFORMANCE

In this section, non-contact isolation performance is quantitatively assessed in the frequency-domain by means of the transmissibility, which is defined in section 3.1. The baseline transmissibility for LUVOIR, using relevant mass properties and conservative coupling assumptions, are given in section 3.2. Finally, section 3.3 examines the sensitivity of the rigid-body transmissibility for change in several of the parameters that participated in the closed-loop dynamics of equation (5).

3.1 Isolation transmissibility as a performance metric

A metric for isolation system performance that is often useful in performing early system-level trades into dynamic stability of large optical telescopes is *transmissibility*. The transmissibility is a frequency-dependent linear transfer function that relates spacecraft to payload motion, in the presence of common disturbances applied to the spacecraft center-of-mass. The payload and spacecraft linear closed-loop dynamics can be written as continuous-time transfer functions in the frequency domain as:

$$\begin{bmatrix} \rho_P(s) \\ \theta_P(s) \end{bmatrix} = H_{PS}(s) \cdot E_S^C(s)\,; \begin{bmatrix} \rho_S(s) \\ \theta_s(s) \end{bmatrix} = H_{SS}(s) \cdot E_S^C(s) \quad (7)$$

In these equations, the payload disturbance are assumed to be equal to zero, for the purposes of computing a transmissibility metric. The 6x6 transfer function matrices $H_{PS}(s)$ and $H_{SS}(s)$ include the effects of closed-loop payload control, relative translation and spacecraft attitude control, and all interface coupling dynamics effects. Substituting $s = j\omega$ in equation (7), eliminating the spacecraft disturbances, one obtains:

$$\begin{bmatrix} \rho_P(j\omega) \\ \theta_P(j\omega) \end{bmatrix} = \underbrace{H_{PS}(j\omega) \cdot H_{SS}^{-1}(j\omega)}_{T(j\omega)} \cdot \begin{bmatrix} \rho_S(j\omega) \\ \theta_S(j\omega) \end{bmatrix} = \begin{bmatrix} T_{\rho\rho}(j\omega) & T_{\rho\theta}(j\omega) \\ T_{\theta\rho}(j\omega) & T_{\theta\theta}(j\omega) \end{bmatrix} \cdot \begin{bmatrix} \rho_S(j\omega) \\ \theta_S(j\omega) \end{bmatrix} \quad (8)$$

The 6x6 transmissibility matrix $T(j\omega)$ is separable into 4 3x3 blocks, as shown in equation (8). In this study, we focus attention on the maximum magnitude of the 3x3 linear transmissibility matrix, $T_{\rho\rho}$, and the 3x3 angular transmissibility matrix, $T_{\theta\theta}$. The maximum magnitude of these transfer function matrices is represented by the frequency-dependent maximum singular value.

3.2 LUVOIR baseline transmissibility performance

To obtain a baseline rigid-body transmissibility for LUVOIR, relevant physical parameters associated with the observatory were used, along with baseline DFP controller designs. For this study, spacecraft and payload mass were assumed to be 3,854 kg and 20,192 kg, respectively; these mass properties are preliminary values available at this early-stage study, and are expected to change as the LUVOIR architecture matures. The observatory orientation associated with the baseline transmissibility assumed a gimbal angle of zero degrees (corresponding to the payload LOS orthogonal to the sunshade plane). To be conservative, the interface cable stiffness based on JWST was used. This estimate is conservative in two important ways. First, LUVOIR is estimated to require much fewer physical power and data cables that bridge the

spacecraft-payload interface. Second, a temperature local to the interface cable bundle of 80K was used in the stiffness matrix; for LUVOIR, the temperature at the interface location is anticipated to be higher, resulting in a lower stiffness. For voice-coil coupling, a coupling matrix was numerically computed from electro-magnetic finite-element modeling software [5], for a custom large stroke/gap voice coil actuator sized for LUVOIR.

Baseline DFP controllers were chosen, based on a study of required LUVIOR repositioning agility and available sensor sample rates. For payload inertial attitude, a PID controller was used, with a bandwidth of 0.5 Hz. For spacecraft attitude control, a PID controller with a bandwidth of 0.03 Hz was sufficient to maintain positive stroke/gap at the interface in the presence of LUVOIR repositioning maneuvers, with necessitating latching of the interface. Finally, interface relative translation control was implemented as a PID controller with a bandwidth of 0.06 Hz.

Figure 6 shows the baseline transmissibility performance for LUVOIR. In Figure 6-a), the linear transmissibility shows unity gain at low frequency which is consistent with interface relative translation control. Note that the damped gain peaking at 0.06 Hz is associated with underdamped PID tuning of this preliminary design, and can be eliminated with more careful relative translation controller design. In Figure 6-b), the angular transmissibility shows broadband vibration isolation, and increasing isolation at low frequencies. The baseline architecture exhibits a peak angular transmissibility of -87 dB, and greater than 110 dB of isolation at frequencies greater than 10 Hz.

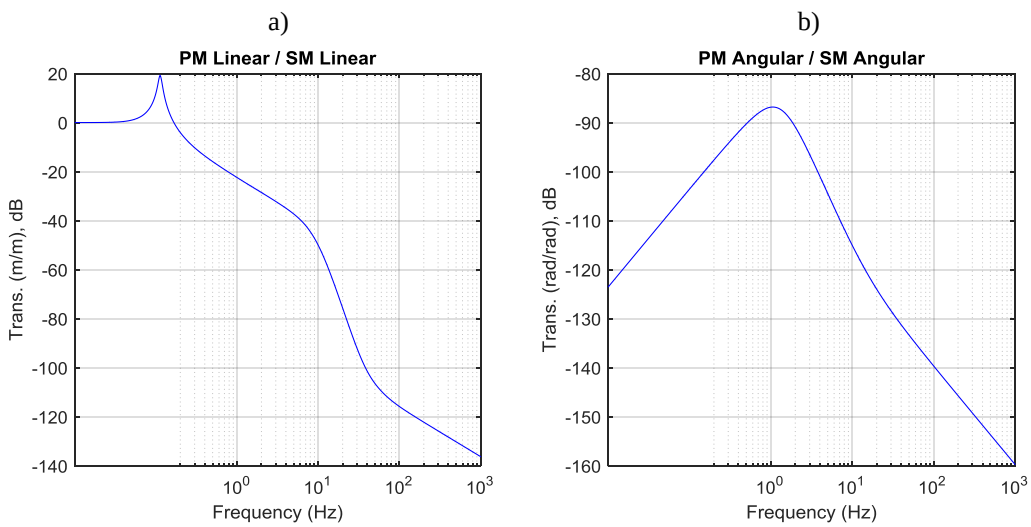

Figure 6. Baseline Transmissibility for the LUVOIR Architecture

3.3 Transmissibility sensitivity studies

In this section, the angular transmissibility performance is studied under variation of the following parameters: payload inertial attitude control bandwidth, actuator damping constant, interface cable stiffness, payload mass fraction, payload geometry knowledge, and gimbal angle.

Figure 7 shows the angular transmissibility sensitivity to variation in payload inertial attitude control bandwidth. Increasing the payload inertial attitude control bandwidth improves the angular transmissivity performance, as shown in Figure 7. Note that payload attitude control bandwidth is ultimately limited at the high end by the payload structural dynamics, which is not modeled in this analysis.

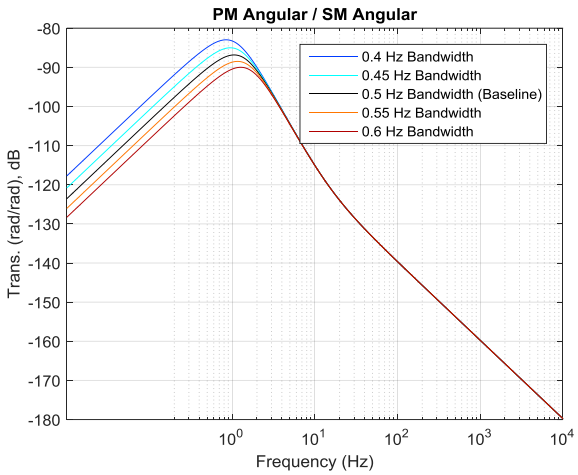

Figure 7. Transmissibility Sensitivity to Pointing Control Parameters

Figure 8 shows the angular transmissibility sensitivity to the interface coupling parameters. Figure 8-a) shows the angular transmissibility sensitivity to variation in the actuator damping constant. The residual damping in the voice coils is primarily due to parasitic currents generated in the actuator. Figure 8-a) shows that increasing actuator damping primarily increases the angular transmissibility in the high frequency regime. Figure 8-b) shows the angular transmissibility sensitivity to variation in the interface cable stiffness. This figure shows that increasing interface cable stiffness primarily increases the angular transmissibility in the low frequency regime.

a) Variation in Actuator Damping Constant

b) Variation in Interface Cable Stiffness

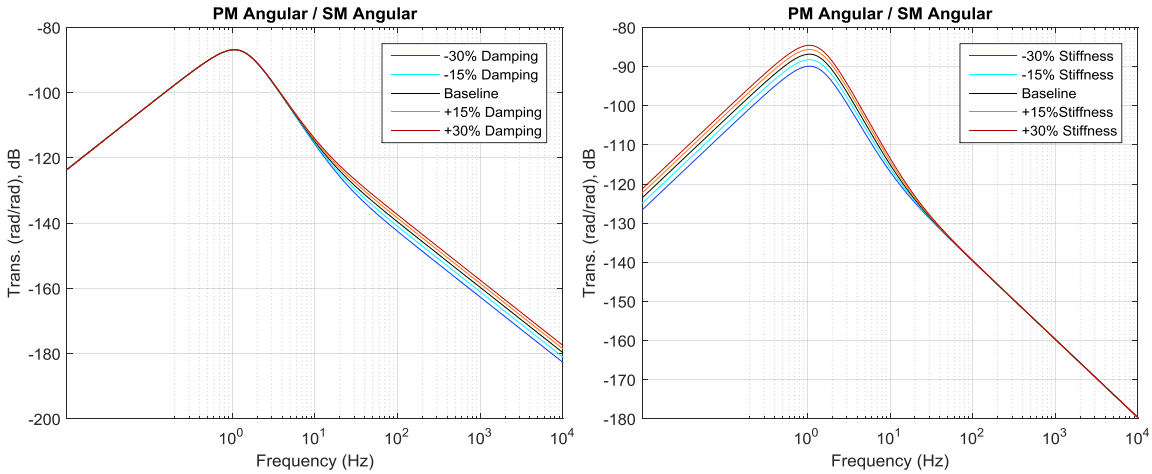

Figure 8. Transmissibility Sensitivity to Interface Coupling Parameters

Figure 9 shows the angular transmissibility sensitivity to the payload mass fraction, which is defined as the percentage of the total system mass (payload plus spacecraft) that is associated with the payload. For this study, it was assumed that changing the mass fraction scaled the payload's mass and inertia properties by a single scalar. Figure 9 shows that increasing payload mass fraction reduces the angular transmissibility.

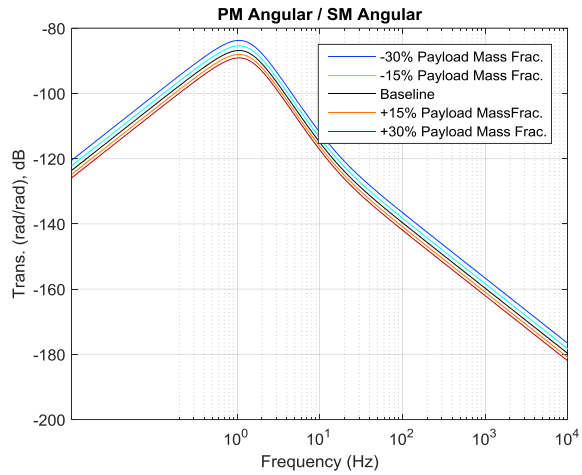

Figure 9. Transmissibility Sensitivity to Payload Mass Ratio

Figure 10 shows the angular transmissibility sensitivity to the payload geometry knowledge in the DFP control law. An error in payload center-of-mass degrades decoupling of relative translational control from payload attitude control. In this study, an error of 10 cm is introduced to the payload center-of-mass in all 3 degrees-of-freedom. Figure 10 shows that knowledge error on the order of 10 cm has negligible effect on the angular transmissibility.

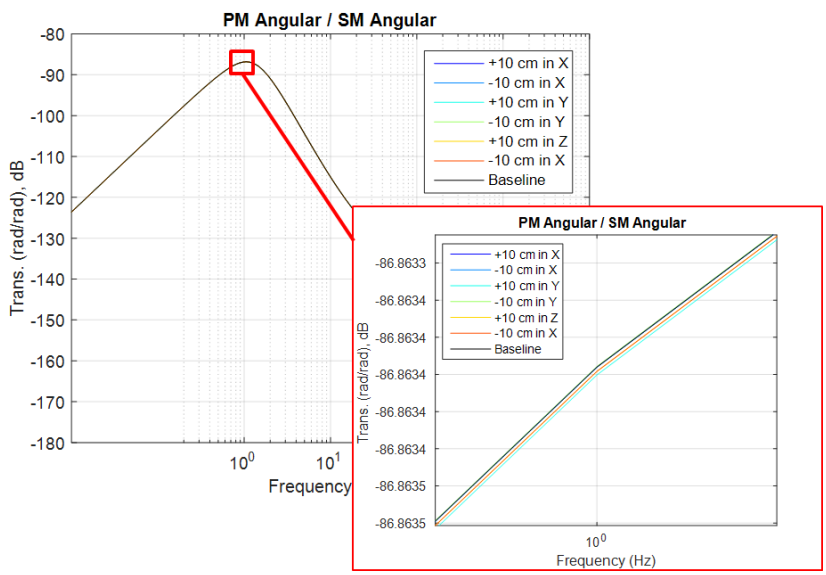

Figure 10. Transmissibility Sensitivity to Payload Geometry Knowledge

Lastly, the angular transmissibility sensitivity is assessed under gimbal angle variation. Spacecraft central inertia matrix, viewed in the payload coordinate frame, is dependent on the payload-spacecraft gimbal angle. In this study, a single axis gimbal is assumed which rotates the payload around the spacecraft S_2 axis. The gimbal allows sunshade to point at the Sun while payload points at a target star. To assess performance sensitivity to variation in spacecraft mass properties, it was assumed that DFP controller parameters are adjusted based on gimbal angle. As Figure 11-a) shows, with controller gains scheduled with gimbal angle, no appreciable angular transmissibility difference is apparent. Figure 11-b) shows that absolute angular transmissivity difference from baseline angular transmissibility, is less than $3x10^{-14}$, with difference largest near the peak of transmissibility.

a) Variation in Gimbal Angle

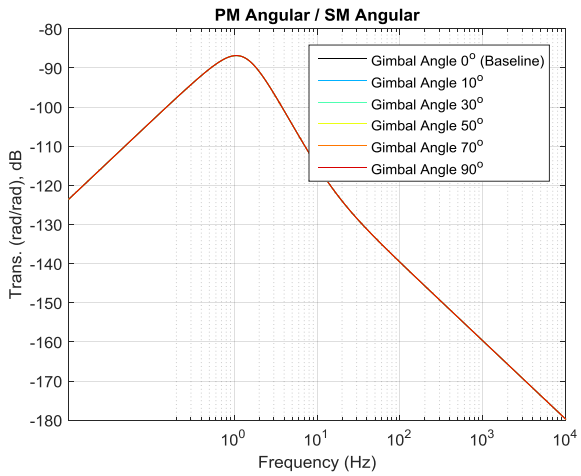

b) Transmissibility absolute difference

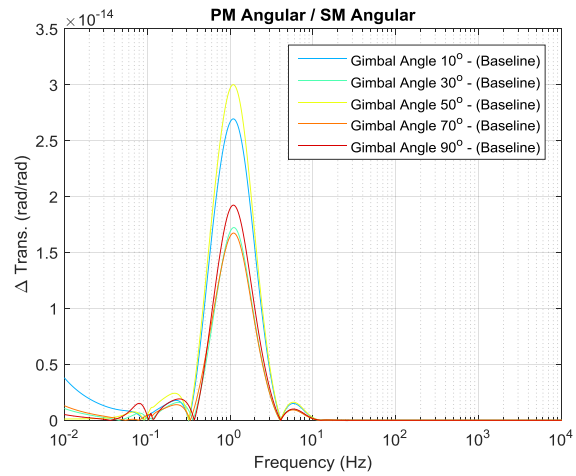

Figure 11. Transmissibility Sensitivity to Observatory Mass Property Variation due to Gimbal Angle

4. CONCLUSIONS AND FUTURE WORK

In this paper, a preliminary analysis of the performance of a non-contact vibration isolation system for the LUVOIR observatory was presented. The isolation system performance was analyzed using linear, rigid-body dynamics, with realistic and conservative linear models of residual coupling effects across the spacecraft/payload interface. Broadband rigid-body angular isolation of greater than -87 dB was computed, with isolation greater than -110 dB for disturbance frequencies greater than 10 Hz. Such broadband isolation is not affected by interface sensing noise, and the high-frequency rolloff is not compromised by any high-frequency isolation structural dynamics, as is typically present in passive isolation systems.

Future collaborative research between Lockheed Martin and NASA Goddard will consider LUVOIR system performance with full spacecraft and payload structural dynamics, and direct computation of observatory performance metrics, such as WFE and LOS angular stability.

REFERENCES

[1] National Aeronautics and Space Administration, Goddard Space Flight Center, "Large UV/Optical/Infrared Surveyor", https://asd.gsfc.nasa.gov/luvoir/ .
[2] Pedreiro, N., "Spacecraft architecture for disturbance-free payload", US Patent 6,454,215 (2002)
[3] Dewell, L. et al, "Precision Telescope Pointing and Spacecraft Vibration Isolation for the Terrestrial Planet Finder Coronagraph", Proc. SPIE 5899 (2005).
[4] Pedreiro, N., "Spacecraft Architecture for Disturbance-Free Payload", J. Guidance, Control and Dynamics, v. 26, N. 5, 794-804 (2003).
[5] ANSYS Maxwell, http://www.ansys.com/products/electronics/ansys-maxwell.